ACS OMEGA

Open Access

http://pubs.acs.org/journal/acsodf

Article

Glycosylated Porphyrin Derivatives for Sonodynamic Therapy: ROS Generation and Cytotoxicity Studies in Breast Cancer Cells

Manita Das,* Vijayalakshmi Pandey, Kuldeep Jajoria, Dhiraj Bhatia, Iti Gupta, and Himanshu Shekhar

Cite This: *ACS Omega* 2024, 9, 1196−1205

Read Online

ACCESS | Metrics & More | Article Recommendations | Supporting Information

ABSTRACT: Sonodynamic therapy (SDT) is a promising alternative to photodynamic therapy for achieving site-specific cytotoxic therapy. Porphyrin derivative molecules have been reported extensively in photodynamic therapy. We have previously shown that the glycosylation of porphyrin-based sonosensitizers can enhance their cellular uptake. However, the sonodynamic potential of these water-soluble glycosylated porphyrins has not been investigated. In this study, we characterized the sonodynamic response of two water-soluble glycosylated porphyrin derivatives. Ultrasound (US) exposure was performed (1 MHz frequency, intensities of 0.05−1.1 W/cm^2) for 0−3 min in continuous mode. Reactive oxygen species (ROS) generation was quantified via ultraviolet−visible (UV−vis) spectrophotometry. MTT assay was used to quantify cytotoxicity caused by sonodynamic effects from these derivatives in the human mammary carcinoma (SUM-159) cell line in vitro. ROS generation from the porphyrin derivatives was demonstrated at a concentration of 15 μM. No significant cytotoxic effects were observed with the sonosensitizer alone or US exposure alone over the tested range of intensities and duration. The free base porphyrin derivative caused 60−70% cell death, whereas the zinc-porphyrin derivative with Zn metal conjugation caused nearly 50% cytotoxicity when exposed at 0.6 W/cm^2 intensity for 3 min. These studies demonstrate the potential of anticancer SDT with soluble glycosylated porphyrins.

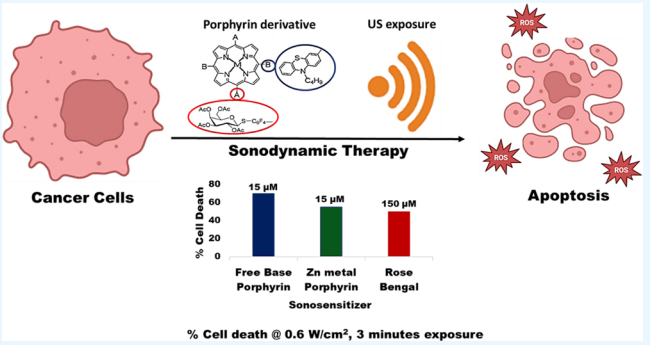

1. INTRODUCTION

Among the subtypes of breast cancer, triple negative breast cancer (TNBC) is characterized by poor prognosis and a higher likelihood of recurrence and metastasis.[1] TNBC is characterized by lack of estrogen receptors (ERs) and progesterone receptors (PRs) and is devoid of human epidermal growth factor receptor 2 (HER2) as well.[2] The heterogeneity of TNBC and absence of well-defined molecular targets make the treatment challenging. Surgery, chemotherapy, and local radiotherapy are the mainstays of TNBC management. In case of advanced and metastatic stages of the disease, an improved approach like poly(ADP-ribose) polymerase inhibitor (PARP)-assisted targeted therapy has demonstrated limited potential in improving the overall survival rates in patients.[3,4] Therefore, developing new therapeutic methods for the treatment of TNBC is an active area of research.

Of the various adjunct therapies developed by researchers, modulation of the intracellular concentration of reactive oxygen species (ROS) has shown potential in cancer therapy.[5,6] Sonodynamic therapy (SDT) is a newer therapeutic approach that is gaining prominence.[7] When specific chemicals called sonosensitizers are combined with ultrasound (US) exposure, they produce ROS that enable a cytotoxic response specifically at the tumor location.[8] SDT is analogous to the clinically approved photodynamic therapy (PDT), in which light is combined with a photosensitizer to produce a cytotoxic effect. Although PDT is clinically effective, it is limited by the depth of penetration of light. SDT is an attractive alternative because it can be used for treating targets deep-seated within the body.[9] Hence, researchers are employing SDT as a potential alternative to light-based PDT because of the capability of the US to activate sonosensitizers.

Researchers have also reported a combination of PDT and SDT for exploiting their synergy.[10−12] A combination of SDT and PDT has been explored for reducing the dosage of both the sensitizers and US exposure or light irradiation[13] to reduce side effects without compromising therapeutic efficacy. The combined therapy is reported to have the potential of inducing apoptosis and autophagy via a decrease in cell migration and mitochondrial membrane potential.[14]

Received: September 26, 2023
Revised: December 4, 2023
Accepted: December 13, 2023
Published: December 29, 2023

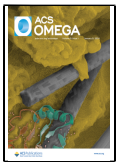

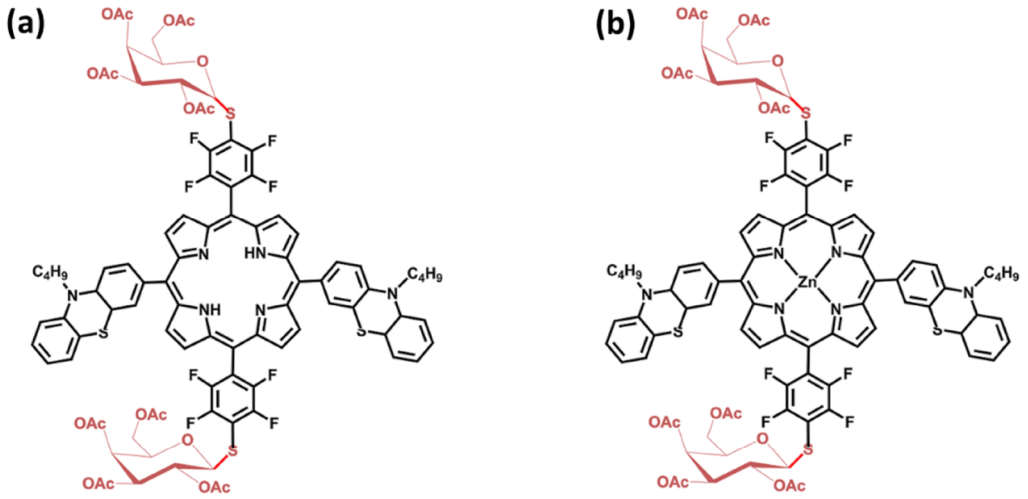

Figure 1. Chemical structures of (a) free base porphyrin and (b) zinc-porphyrin having thiogalactose sugars (shown in red) used in this study.

The therapeutic effects of SDT can be controlled by tuning US exposure parameters such as the amplitude and duration. Acoustic cavitation, or the growth and collapse of bubbles in response to US, is a dominant mechanism of ROS generation in SDT. In addition to activating sonosensitizing agents for ROS generation, US insonification in SDT also generates cavitation and shear stress.[15] This mechanical effect enhances membrane permeability by sonoporation and can have a synergistic anticancer effect. The sonoporation effect of cavitation can also enhance tumor regression versus conventional treatment.[16]

Of the various classes of sensitizers known, porphyrin derivatives are the most studied in PDT due to their low dark toxicity and selective accumulation in tumors. Although certain drugs are clinically approved for PDT, they are associated with notable limitations. For instance, drugs like Foscan (Biolitec Pharma Ireland Ltd.) and Photofrin (Concordia Laboratories Inc., US) are known for affecting healthy tissues owing to their nonspecificity.[17,18] Further, a palladium bacteriochlorin-a porphyrin-based sensitizer is hydrophobic and therefore has relatively long retention times in tissues.[19,20] To address these shortcomings, Gupta and co-workers have developed novel porphyrin derivatives via carbohydrate functionalization.[21] These molecules are trans-A_2B_2 porphyrins chemically modified via glucose functionalization and therefore have a better solubility in water. The rationale behind this modification was that the malignant cells are known to overexpress carbohydrate-binding proteins. The glucose functionalization on these molecules assists them in specifically targeting the tumor by carbohydrate-binding lectins via receptor-mediated endocytosis. They also observed that these porphyrins have high solubility and cellular uptake. Colocalization studies carried out in A549 lung cancer cell lines revealed significant endoplasmic localizations especially of the Zn-metalated derivatives as well as partial colocalization in lysosomes and mitochondria. These porphyrin derivatives with Zn metal conjugation showed good PDT activity and ROS generation in human breast cancer cells via an effective type-I photo reaction. However, the sonodynamic potential of these agents has not been previously evaluated, which was the focus of the present study. Specifically, we employed two derivatives from this class of compound (free base porphyrin derivative and its Zn metal complex, shown in Figure 1) and evaluated their sonodynamic response in vitro in a triple negative breast cancer cell line.

2. MATERIALS AND METHODS

2.1. Materials. Rose Bengal (RB, $C_{20}H_2Cl_4I_4Na_2O_5$) was procured from Alfa Aesar; thio-glycosylated *trans*-A_2B_2-type porphyrin and its Zn metal complex were synthesized at IIT Gandhinagar. 1,3-Diphenylisobenzofuran (DPBF) and phosphate-buffered saline (PBS, 10× solution, pH 7.4) were procured from Sigma-Aldrich. Dimethyl sulfoxide (DMSO) was procured from SRL. 3-(4,5-Dimethylthiazol-2-yl)-2,5 diphenyltetrazolium bromide (MTT) was procured from Invitrogen.

2.1.1. Synthetic Protocol for Free Base Porphyrin. The novel porphyrin molecules were synthesized and characterized in Prof. Iti Gupta's Lab at IIT Gandhinagar. The detailed synthesis scheme and characterization were previously reported.[21] Briefly for the synthesis of prophyrins, glycosylated dipyromethane (0.07 mmol, 1.5 equiv) and aldehydes (0.05 mmol, 1 equiv) were dissolved in DCM (4 mL) and stirred for 2 min. Later, trifluoroacetic acid (10 μL, 2.6 equiv) was added. The resulting reaction mixture was stirred at room temperature under an inert atmosphere (nitrogen) for 9 h in the dark. Later, 2,3-dichloro-5,6-dicyano-1,4-benzoquinone (DDQ, 0.15 mmol, 3.0 equiv) was added, and the reaction mixture was stirred under air for 2 more hours. The reaction progress was monitored via TLC, and 80% DCM/hexane was used as the mobile phase. The formation of porphyrin was confirmed by the appearance of a brown color spot on TLC. The product was purified using neutral alumina column chromatography, and the desired molecules were eluted using 80% DCM/hexane as the solvent.

2.1.2. Synthetic Protocol for Zinc Porphyrin. Free base porphyrin (1 equiv) was dissolved in DCM (20 mL), and zinc(II) acetate (1.2 equiv) dissolved in chloroform (15 mL) was added to it. The reaction mixture was stirred for 4 h under a nitrogen atomosphere. The formation of the desired product was indicated by a polar green spot of zinc porphyrin on silica TLC. The pure zinc porphyrin was obtained by neutral alumina column chromatography using a 100% DCM/hexane mixture.

The structural confirmation of product formation and molecular weight determination was done using ^{19}F NMR,

https://doi.org/10.1021/acsomega.3c07445
ACS Omega 2024, 9, 1196−1205

MALDI-MS, and FTIR. Also, the spectral properties of the molecules were determined by recording the UV−vis absorption spectra and fluorescence studies (as reported in Pandey et al.).

A stock solution of 1.52 mM ROS scavenger (DPBF) and 0.52 mM SS (standard-RB and novel-porphyrin derivatives) in DMSO was prepared. The solution was transferred to amber vials and sealed with Teflon and parafilm tape to avoid any degradation due to light. The solution was stored at −20 °C for future use and thawed to room temperature before use.

2.2. US Treatment. The US exposure was performed using an apparatus consisting of an US system equipped with a 1 MHz probe (Physiogears, Chennai, India). The transducer had a 35 mm aperture diameter, and a focal length of 20 mm was used. The probe was calibrated in the free field at 1 MHz at a distance of 4 mm from the transducer aperture by using a 1 mm diameter needle hydrophone (NH 1000, Precision Acoustics, Dorchester, UK). The 4 mm distance was considered taking into account 1.5 mm of the cell well plate and a nearly 2 mm thickness of intervening US gel. The spatial average temporal average intensity was computed after considering the attenuation of US at 1 MHz through the cell well plate. The US transducer was positioned in the vertical direction in the probe holder such that the transducer aperture was facing upward. For subjecting the reaction to US exposure, US gel was applied to the transducer, and a 35 mm Petri dish containing the sonosensitizer solution was placed on it. The US exposure parameters used were as follows: 1 MHz frequency, 100% duty cycle. The intensities and exposure times ranged from 0.05 to 1.1 W/cm^2 for 0−3 min, respectively. When this approach is translated to in vivo studies, we plan to use a focused transducer for site-specific targeting. We reported acoustic intensities in the present study. The US system used in this study also provided the intensity values on its interface/dials. However, the US intensity can vary with spatial distance and the position of the beam. As the cell well plate was located close to our transducer surface (4 mm in the near field) in our experiments, we calibrated the field close to the surface of the transducer for our experiments. Our quantitative hydrophone measurements indicate that the nominal intensity listed on the US system's buttons was likely calibrated at the Rayleigh distance of the transducer (30 mm) and is thus not relevant for the present study.

2.3. Instrumentation. The UV−vis absorption studies were conducted using a Shimadzu UV 1800 spectrophotometer, recording the spectra in continuous scan mode in the wavelength range of 200−900 nm in steps of 1 nm. The absorbance for the MTT assay was recorded with a multiplate reader (Bio-Tek multiplate reader) at 570 nm.

2.4. Evaluation of US-Mediated ROS Generation. Singlet oxygen ($^1O_2$) is the dominant species that prevail and cause cytotoxicity.[21] In this study, the assessment of US-mediated singlet oxygen generation from a similar porphyrin derivative and its Zn complex was made in aqueous media. For analyzing the US-triggered ROS generation from the novel sonosensitizers, a chemical trap method was employed, in which DPBF acted as the scavenger of singlet oxygen species. The choice of DPBF as the ROS scavenger was made based on previously reported work that demonstrated the capability of DPBF to efficiently capture singlet oxygen species that is dominantly produced with these porphyrin derivatives. Porphyrin derivatives are known to generate singlet oxygen as the dominant ROS via a type II pathway when irradiated with light.[22] Previous studies with Zn-metalated porphyrins suggest that singlet oxygen will be the main ROS species when SDT is performed.[23] It may be challenging to use DPBF in complex biological systems as a $^1O_2$ detector due to the presence of other free radicals. However, in a controlled environment such as that employed in this study, DPBF has been reported by us[21] and others[24−26] for measuring $^1O_2$. Further, species other than $^1O_2$ are challenging to detect in solution. We will employ techniques such as EPR in our future studies to investigate other ROS generated, if any, during the US exposure of our sonosensitizer. The ROS generation was compared to that of RB, a well-characterized sonosensitizer. UV−vis spectrophotometry was used to monitor the spectral changes of DPBF in response to its interaction with ROS. Baseline correction was performed by using Milli-Q water prior to the actual measurements. Next, the absorbance of sonosensitizers was fixed at 0.5 and that of DPBF was fixed at 1.0, and their effective concentrations were calculated from the stock solutions. For the standard RB, its DMSO solution showed an absorption peak that was observed at 540 nm. First, a control UV−vis spectra scan was run on a sample containing a scavenger molecule added to a solution of the sonosensitizer in order to assess the stability of the molecules in the absence of US exposure. The solution showed characteristic absorption maxima at 540 nm corresponding to RB and at 510 nm as well as at 324 nm corresponding to DPBF. Later, sham measurements were also performed using the concentrations of RB and DPBF as mentioned above by placing the solution-filled Petri dish over the transducer without turning it on. This measurement served as a negative control. US exposure was given with a physiotherapy transducer of 1 MHz center frequency having a 35 mm aperture diameter, and a focal length of 20 mm was used. The US exposure was given over a range of intensities and varying exposure times. The singlet oxygen generated due to sonosensitization of porphyrin reacts with DPBF to form an endoperoxide 1 which then decomposes to 1,2-dibenzoylbenzene (DBB).[25] This causes a decrease in the intensity of the absorption band corresponding to DPBF at 324 nm, which was monitored using a UV−vis spectrophotometer.

The ROS generation was evaluated from both the novel porphyrin derivatives in response to US exposure using the same protocol. For the mixture of the solution containing DPBF and porphyrin, peaks were observed at 324 and 516 nm, respectively, as reported previously by Pandey et al. Since the characteristic peak of the porphyrin derivatives at 516 nm overlaps with the absorption maxima of DPBF at 510 nm, therefore, to ascertain the singlet oxygen generation, the decrease in the absorption at 324 nm was analyzed.

2.5. Quantum Yield Calculation. The quantum yield of ROS generation for novel porphyrins was calculated by using RB as the standard in DMSO as reported previously.[27,28] Briefly, for the experiments, DPBF with a fixed concentration of 98 μM was prepared in the dark and was protected from stray light exposure. The absorbance was fixed at 0.6, and the effective concentrations for standard RB and porphyrin were calculated from the stock solutions. The absorbance for RB and porphyrin was recorded, and the decay in absorbance was plotted at 324 nm to obtain the slopes. The quantum yield of ROS was calculated as

$$\Phi_{\Delta(S)} = \Phi_{\Delta(S0)} \times \{\text{slope}(S)/\text{slope}(S_0)\} \quad (1)$$

https://doi.org/10.1021/acsomega.3c07445
ACS Omega 2024, 9, 1196−1205

where S is the slope obtained from porphyrin and S_0 is the slope obtained from RB.

2.6. Cell Culture. Human breast cancer cells (SUM159) were cultured in Hams-F12 media and 5% fetal bovine serum (FBS), 10 μg/mL insulin, 10 μg/mL dihydrocortisone, and 100 U/mL penicillin−streptomycin, incubated at 37 °C in a 5% CO_2 atmosphere with 90% humidity. The cells were grown in T25 flasks, and they were harvested with trypsin/EDTA once the flask achieved 90% confluency. For the experiments, the cells were seeded in 6-well plates with a density of 1−1.5 × 10^5 cells/mL and incubated for 48 h at 37 °C in 5% CO_2 prior to treatment. Post 24 h incubation, RB (150 μM) was added to selected wells and further incubated at 37 °C for 2 h with O_2/CO_2/air (20:5:75, v/v/v), following which the media was removed and washed with 200 μL of PBS buffer (pH-7.4). Each well was filled with fresh SFM and subjected to US exposure. The media was changed post US exposure, and cell viability was analyzed using the MTT assay. The same protocol was followed when free base porphyrin (15 μM) and metalated porphyrin (15 μM) were evaluated as sonosensitizers. The glycosylation of the porphyrin derivatives used in this study enhances its solubility in water. However, to ensure complete solubility, sparing amount of DMSO is typically used. The concentration of DMSO (<5%) used for sample preparation is so low that it cannot exert cytotoxic effects on the cells, as observed from the previous study by Pandey et al. This approach also aligns with previously reported literature wherein studies have been carried out for evaluating photodynamic effect-mediated cytotoxicity using sensitizer molecules dissolved in DMSO.[29−31]

2.7. MTT Assay. Briefly, 5 min after the treatment, the SF medium was removed, and 0.5 mg of MTT in 1 mL of media was added to the wells containing treated cells. The cells were incubated for 2 h at 37 °C with O_2/CO_2/air (20:5:75, v/v/v). After incubation, the solution was removed, and 1 mL of DMSO was added. The cells were then incubated for an additional 5−10 min, and then the absorbance was recorded at 570 nm using a multiplate reader. The proportion of viable cells for treatment was calculated from the values obtained with reference to the control group.

2.8. Scratch Assay. The effect of the uptake of SDT on collective cell migration was analyzed using a scratch assay. SUM-159 cells were used in this study. For the experiments, the cells were grown in 6-well plates, and at 100% confluency, a scratch was made using a 200 μL tip. The closure of this wound under various treatment conditions was analyzed. The treatment groups consisted of control with no treatment and cells treated with only RB, free base porphyrin, and Zn porphyrin alone. The effect of US exposure alone at 0.3 and 0.6 W/cm^2 of exposure for 3 min on the wound closure was also assessed. For the SDT treatment groups, the sonosensitizer concentration was 15 μM, and US exposure was performed using the same intensities. The cells were observed immediately after the treatment, and images were acquired using the bright-field mode of the Nikon fluorescence microscope; this observation has been termed as 0 h. Later, the cells were observed, and imaging was done at 12 and 24 h.

2.9. ROS Generation DHR Assay. The ROS generation within cell SDT was estimated using dihydrorhodamine (DHR). This assay employed a nonfluorescent molecular probe, DHR, that generates a fluorescent compound rhodamine 123, a fluorescent compound upon oxidation when ROS are produced. Intracellular ROS generation was monitored via fluorescence microscopy. For visualization of ROS generated, DHR was excited at 488 nm, and the emission was observed in the range of 500−540 nm (green region) using a fluorescence microscope. The ROS generation was assessed in treatment groups where cells were subjected to SS alone, US alone, and SDT.

For these measurements, SUM-159 cells were dosed with 15 μM concentration of the sonosensitizer (RB, free base porphyrin, or Zn porphyrin) and incubated for 2 h. In the group where SDT was given, after 2 h of incubation, the cells were exposed to US at 0.3 and 0.6 W/cm2 intensity for 3 min. After the treatment, the cells were stained with a 2.5 μM concentration of DHR 123 (DHR) for 30 min at 37 °C. Subsequently, the cells were fixed with 4% PFA and mounted on slides using nuclear stain DAPI. The fixed cells were imaged using the 40X objective of fluorescence microscope by exciting DHR at 488 nm and receiving the emission in the range of 500−540 nm. The micrographs of cells are represented as composite images of DHR (green fluorescence, showing the presence/absence of ROS generation) and DAPI (blue fluorescence, showing a nuclear morphology).

2.10. Statistical Analysis. GraphPad Prism 9.3.1 was used to analyze the data and plot graphs. All data are expressed as the mean ± standard deviation of 5 independent experiments. The variations between the groups were analyzed using a one-way analysis of variance (ANOVA), and post hoc comparison between groups was performed using the Tukey's honest significance difference test.

3. RESULTS

3.1. Singlet Oxygen Generation via the Sonodynamic Effect. The molecular structures of the novel porphyrin molecules are shown in Figure 1.

The UV−vis spectral changes shown in Figure 2a demonstrate no change in the absorbance of DPBF when the porphyrin solution was subjected to sham, suggesting that

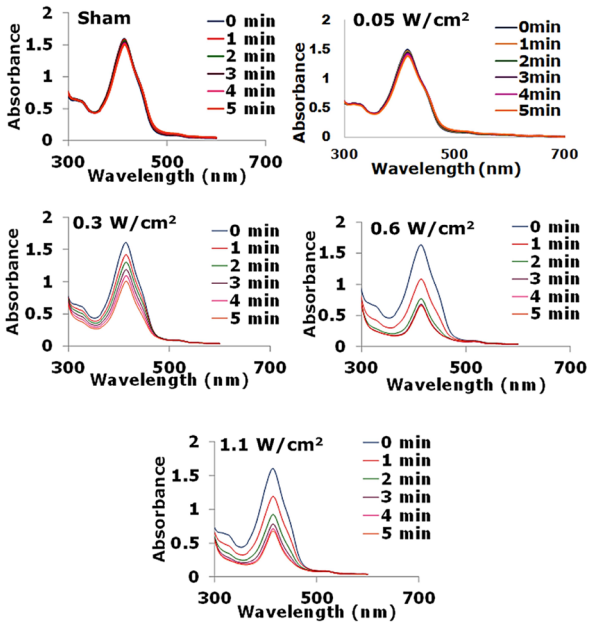

Figure 2. Comparison of UV−vis spectra of the 12 μM porphyrin solution containing 98 μM DPBF subjected to sham and US exposure at varying power intensities (0.05, 0.3, 0.6, and 1.1 W/cm^2).

https://doi.org/10.1021/acsomega.3c07445
ACS Omega 2024, 9, 1196−1205

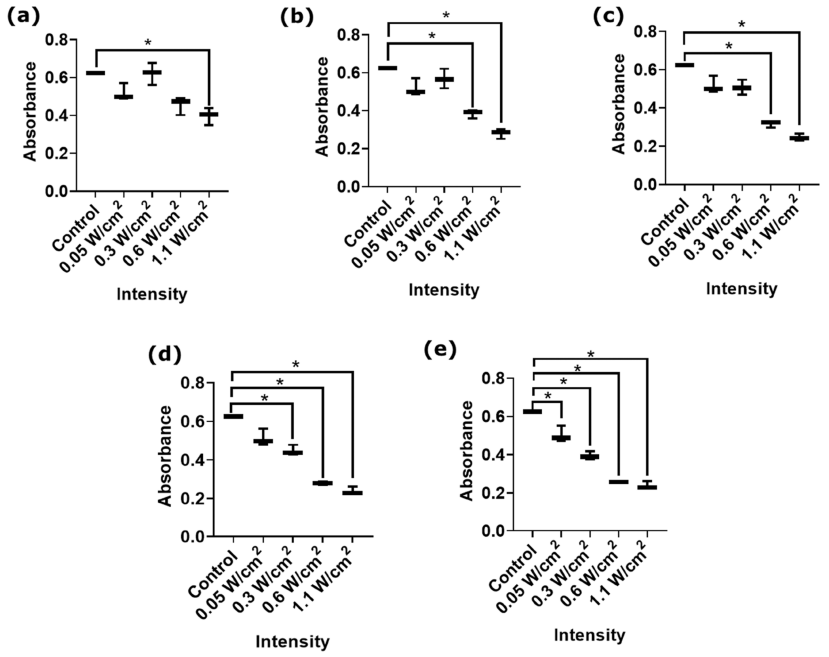

Figure 3. Bar plots showing quantification of singlet oxygen generated at various intensities for exposure of (a) 1, (b) 2, (c) 3, (d) 4, and (e) 5 min.

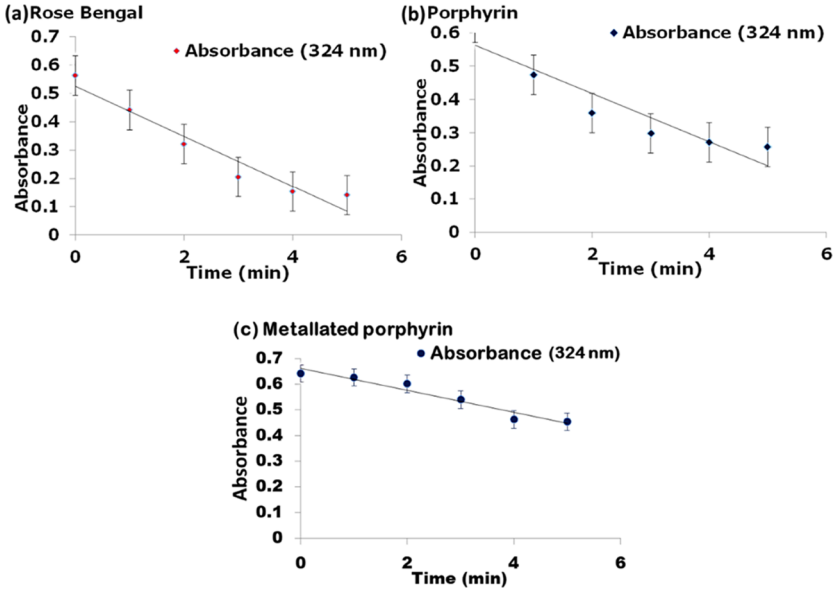

Figure 4. Rate of decrease in absorption values at 324 nm upon sonosensitization of (a) RB, (b) porphyrin, and (c) metalated porphyrin at 0.6 W/cm^2. The concentrations of solutions were DPBF (98 μM), porphyrin and metalated porphyrin derivative (12 μM), and RB (14 μM).

ROS generation does not take place. US exposure in the absence of a sonosensitizer did not generate detectable levels of ROS for the US intensities used in the present study (Figure S1).

However, upon exposure to the US, there is a decrease in the absorbance of DPBF indicative of ROS generation caused by a sonodynamic effect (as shown in Figure 2b−e). We observed that the ROS generation is dependent on the US intensity. The ROS generation was quantified and presented in the form of bar plots (Figure 3).

The quantification suggested that an US intensity of 1.1 W/cm^2 caused a significant ROS generation at 1 min of exposure (Figure 3a), and at 0.6 W/cm^2, 2−3 min of exposure is required to cause significant ROS generation (Figure 3b,c). For an even lower intensity exposure of 0.3 W/cm^2, a significant singlet oxygen production was seen at 4 min of exposure (Figure 3d). It was observed that exposure of even 5 min did not aid in the generation of a significant quantity of ROS (Figure 3e).

3.2. Quantum Yield of Singlet Oxygen Generation.

The quantum yield of singlet oxygen generation of the novel porphyrin derivatives was calculated by employing RB as the reference sonosensitizer RB (Φ_Δ = 0.76 in DMSO) using DMSO as the solvent. The absorption data obtained at an US intensity exposure of 0.6 W/cm^2 was fitted to eq 1, and the quantum yield was found to be 0.59 ± 0.05 for the free base porphyrin (Figure 4) and 0.39 ± 0.02 for the zinc derivative.

https://doi.org/10.1021/acsomega.3c07445
ACS Omega 2024, 9, 1196−1205

3.3. In Vitro Studies. *3.3.1. Cell Viability Assay.* The effect of SDT on the cell viability of SUM 159 cells analyzed via the MTT assay is demonstrated in Figure 5. The results revealed

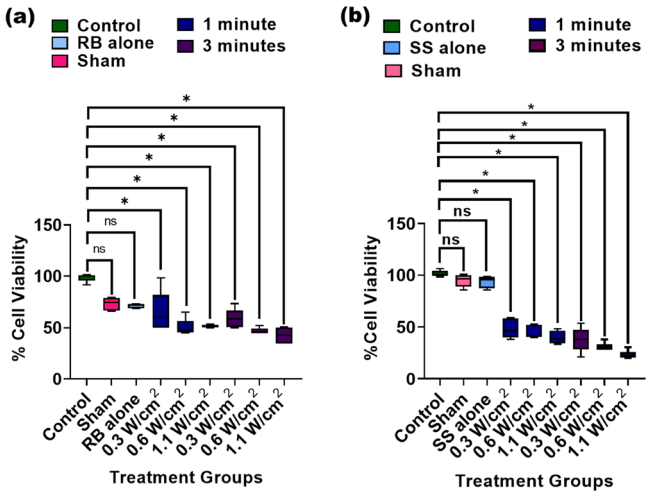

Figure 5. Bar plots showing cell viabilities on subjecting them to SDT using (a) RB & and (b) novel porphyrin as the sonosensitizer. $N = 5$, * represents $p < 0.05$.

no cytotoxic effects of US exposure alone over the tested range of power intensities and time, as shown in Figure S2. The effect of SDT using RB as the standard is shown in Figure 5a. The studies carried out for quantification of ROS generation revealed that a 15 μM free base sonosensitizer was required for significant ROS generation. Therefore, this concentration was selected for reporting the in vitro evaluations. For a fair comparison of the sonodynamic effect, the concentration of metalated porphyrin was also kept at 15 μM. The cyan colored bar plots in Figures 5b and 6c corresponding to free base and metalated porphyrin revealed that both the sonosensitizers at the selected concentration did not induce any cytotoxic effects

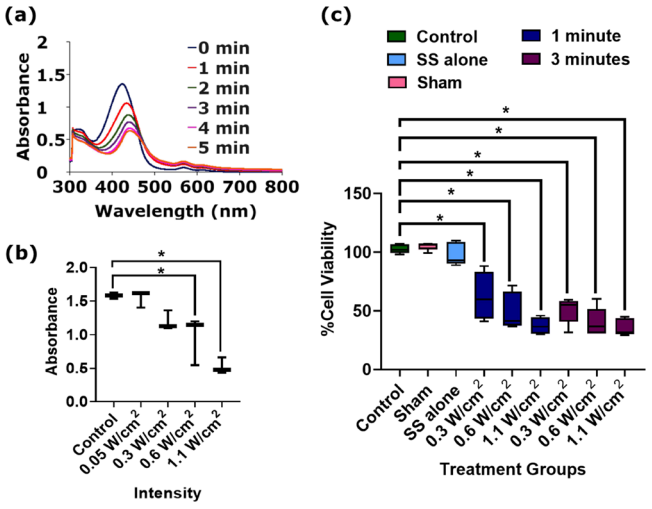

Figure 6. (a) Comparison of UV−vis spectra of the 17 μM metalated porphyrin solution containing 98 μM DPBF subjected to US exposure at 0.6 W/cm^2 intensity, (b) quantification of singlet oxygen generation for an exposure of 3 min $N = 5$, * represents $p < 0.05$, and (c) bar plots showing cell viabilities post SDT using metalated porphyrin (15 μM) as the sonosensitizer. $N = 5$, * represents $p < 0.0001$.

to the cancer cells. The cell viabilities are ∼99% for both of these sonosensitizers. Later, the cells were subjected to sham (negative control), the pink-colored bar plots in Figures 5b and 6c represent this treatment group, and the results showed ∼100% cell viability for both the novel sonosensitizers.

The singlet oxygen generation studies indicated no significant ROS generation at 0.05 W/cm^2, and therefore, for the in vitro experiments, this intensity was skipped. The cells were subjected to intensities of 0.3, 0.6, and 1.1 W/cm^2 over a time interval of 1, 3, and 5 min. We did not proceed beyond 1.1 W/cm^2 intensity because the preliminary investigations showed that the cells get detached from the surface on subjecting to an intensity greater than 1.1 W/cm^2.

The effect of SDT using free base porphyrin is shown in Figure 5b. Cytotoxicity was caused at the investigated US intensities. At 15 μM concentration, 45−55% of cell death was observed over the tested intensities when exposed for 1 min. The cell viability dropped further 60−70% when the exposure time was increased to 3 min. Further increase of exposure time to 5 min did reduce the cell viability, but a temperature rise was also observed under these conditions. Under these conditions, it is anticipated that thermal effects will also affect cell viability, and the cell death will not be purely due to the sonodynamic effect. With these observations, we identified 0.6 W/cm^2 of US exposure for 3 min as well-suited for therapy.

Similarly, the sonodynamic effect of metalated porphyrin at 15 μM is shown in Figure 6c. The results indicated <50% of cell death over all the three tested values of intensities when exposed for 1 min. On increasing the time of exposure to 3 min, the cell viability dropped to approximately 50%.

Both porphyrin derivative sonosensitizers showed higher cytotoxic effects as compared to the standard sonosensitizer (RB) (Figure 5a), which showed comparable cytotoxicity to the metalated porphyrin even at 10 times higher concentrations (150 μM). The comparison of cellular viability assays indicates that free base porphyrin demonstrated the highest cytotoxic effects among the sonosensitizers tested.

3.3.2. Wound Healing Assay. The effect of SDT on cell migration was evaluated via a scratch assay. As shown in Figures 7 and 8, it was observed that cells in the control group migrate, which is evident from the presence of live cells in the scratched area post 24 h of treatment. The treatment of the cells with SS alone does not allow cell migration (Figure S3), which is an interesting finding. US exposure alone allows the cells to migrate (Figure S4), showing that these exposure intensities are mild. Interestingly, 24 h after exposure to SDT in addition to the loss of migration ability, the cells in the unscratched areas were observed to be under stress. This is evident from the loss of cell density in the unscratched areas as well as the presence of debris in the cell well plates (also seen in the microscopic images). The loss of cell viability is more pronounced in the treatment groups subjected to SDT at 0.6 W/cm^2 of intensity. These results suggest that SDT imparts irreversible damage to the cells, affecting their migration and proliferation rates 24 h post treatment. SDT also prevents cell migration, which is a desirable effect to stop tumor invasion. Although further studies are needed to assess what additional effect SDT has on the sensitizer alone in limiting cell migration, these results add to the insights obtained with cell viability and microscopy studies.

The presence of dead cells corroborates the MTT assay results wherein cytotoxicity after SDT is being observed.

https://doi.org/10.1021/acsomega.3c07445
ACS Omega 2024, 9, 1196−1205

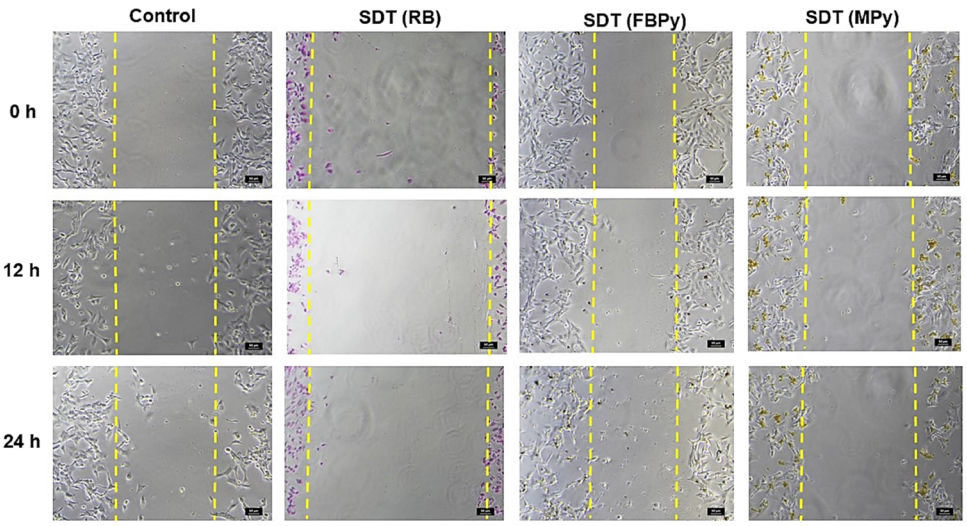

Figure 7. Bright-field microscopy images taken at different time points using a Nikon camera showing the migration of SUM-159 cells in groups subjected to SDT with a sonosensitizer concentration of 15 μM and an US intensity of 0.3 W/cm^2 for 3 min.

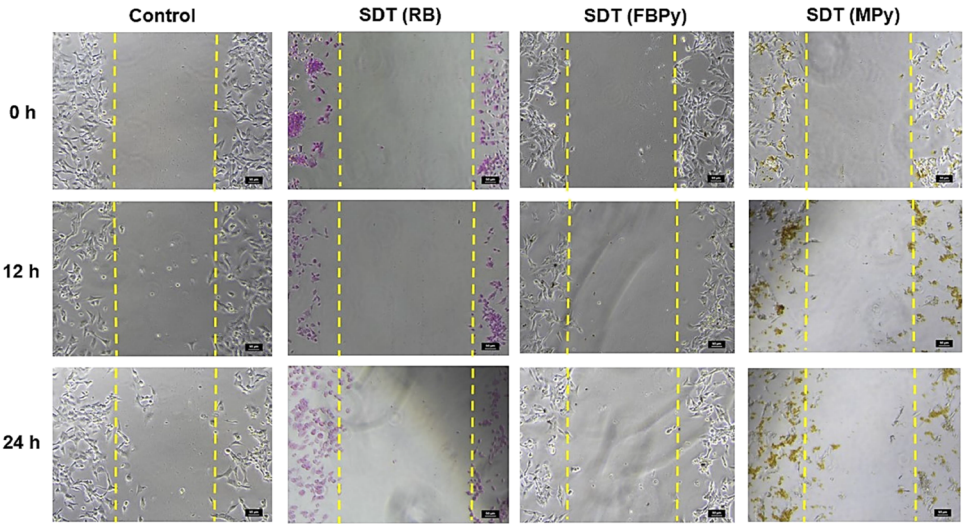

Figure 8. Bright-field microscopy images taken at different time points using a Nikon camera showing migration of SUM-159 cells in groups subjected to SDT with a sonosensitizer concentration of 15 μM and an US intensity of 0.6 W/cm^2 for 3 min.

3.3.3. Intracellular ROS Generation. Figure 9 shows intracellular ROS generation observed using fluorescence microscopy and the molecular probe DHR. In the untreated control group, no ROS generation was apparent, which is evident from the absence of green fluorescence in the cells, and thus, only the nucleus is visible from DAPI staining. Similarly, in the groups dosed with only sonosensitizers or only US exposure, ROS generation was not observed (Figure 9, rows A and B). However, in the groups where SDT was performed (Figure 9, rows C and D), ROS generation was apparent from the green fluorescence emanating from the cells. With the novel porphyrin molecules as the sonosensitizers, cell death was more prominent, which can be observed from the agglomerated dead cells showing fluorescence due to ROS generation.

4. DISCUSSION

While the fundamental processes of PDT are well recognized, the relative contributions of the multifaceted mechanisms of SDT are still being investigated. Acoustic cavitation is recognized as a dominant mechanism for the sonodynamic effect.[32,33] It can activate the sonosensitizer, which leads to the generation of ROS. Sonoluminescence, a process in which light is formed when a solution is irradiated with US, is another likely mechanism for ROS generation.[23,34] Under the appropriate insonation conditions, gas bubbles can be nucleated. While the gas bubbles undergoing inertial cavitation grow and expand to a maximum size before collapsing, the bubbles undergoing stable cavitation oscillate, imparting a mixing effect on the surrounding media.

Within the tumor microenvironment, the energy generated by these disintegrating bubbles can cause the formation of sonoluminescent light, triggering the electrons in the ground state of the sonosensitizer to move to an excited state.[35] When the excited electron returns to its stable ground state from the transient excited state, the energy released can assist the formation of ROS from the oxygen molecules present. The cellular damage has been linked to the generation of oxygen ion, peroxide, and singlet oxygen species, and in some instances, deeper damage is caused due to the generation of

https://doi.org/10.1021/acsomega.3c07445
ACS Omega 2024, 9, 1196−1205

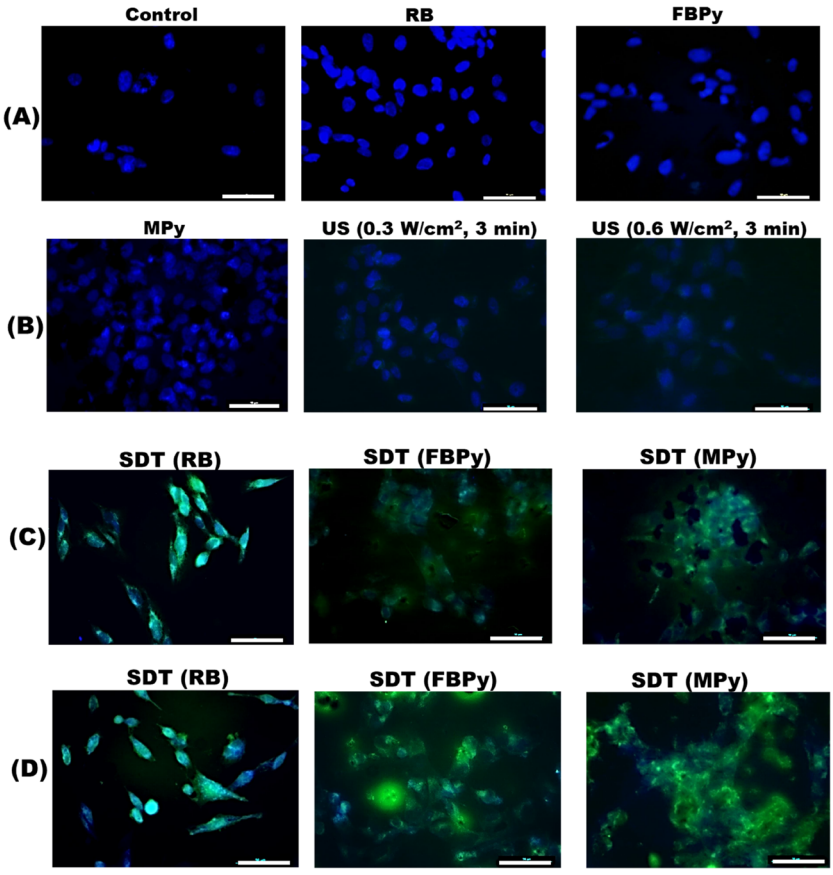

Figure 9. Fluorescence microscopy images of cells in various treatment groups from DHR staining studies performed to visualize intracellular ROS generation in SUM-159 cells. Cells were treated with DHR (green, to detect ROS for 30 min). The cells were fixed, stained with DAPI (blue, to stain the nucleus), and observed with a 40× objective. The images in rows A and B represent control group and the treatment groups where the cells were subjected to exposure with either only SSs or US. The images in rows C and D represent groups where the cells were subjected to SDT. Images in row C correspond to SDT with an US exposure at 0.3 W/cm^2 intensity and in row D at 0.6 W/cm^2 intensity. The scale bar is 50 μm.

alkoxy and peroxy free radicals.[36,37] The cytotoxicity of free radicals such as OH and H produced during bubble collapse was linked to their oxidative capability. In addition to these, ROS may also be generated via direct pyrolysis of the sonosensitizer or water molecules reacting with dissolved oxygen when subjected to an US trigger.[38,39]

Despite recent advances in the regime of developing SDT as an adjunct therapy, advances are needed in developing sonosensitizers, identifying the correct US exposure regimen, and providing image guidance to translate this therapy to the clinic. Toward this development, the current work reports the sonodynamic potential of a water-soluble carbohydrate-functionalized porphyrin derivative in causing cytotoxicity to triple negative breast cancer cells. The choice of cell line for this study was motivated by two primary factors: (i) the need for the development of new therapeutic strategies for triple negative breast cancer owing to the absence of receptors that make the treatment difficult and (ii) there is an increased metabolic activity found in TNBC cells and a higher number of glucose transporters that assist enhanced cellular internalization of sugar-linked porphyrin moieties.[40,41]

Pandey et al. reported a high cellular uptake, ROS generation efficiency, and photodynamic efficacy of water-soluble thioglycosylated zinc(II) porphyrins relative to that of the corresponding nonmetalated derivatives. However, we observed a reversal in these trends when similar derivatives were experimented for SDT. This is indicative of the basic difference in the cell death mechanisms underlying both of these therapies.

The primary limitation of our work is the difficulty in evaluating the standing wave generation and possible multiple reflections during the in vitro experiments. The reported intensities were measured in the water tank in the presence of the cell well plate but did not factor in the standing waves. The experimental setup and geometry of the cell culture dish contribute to the standing wave phenomenon. Also, it is challenging to recreate the exact in situ parameters during the experiments. However, the reproducible results and careful measurement of downstream effects such as ROS suggest consistency in the studies that were carried out. Future studies can be conducted by using cavitation nuclei like microbubbles or nanodroplets, and the therapeutic effect can be enhanced. Cavitation detection can be incorporated to assess and quantify cavitation. Although our findings showed no effect of only the US exposure on cell viability, long-term effects on cell viability and proliferation need further investigation. In addition to this, previous studies by Pandey et al. showed the enhanced uptake of these moieties in A549 (lung cancer) cells. A limitation of the present study is that we did not show improved uptakes specifically in TNBC cells. Whether glycosylation improves therapeutic efficacy can be assessed only through in vivo studies, which would be the subject of future work. Nonetheless, as long as a sufficient concentration of the sonosensitizer accumulates in the tumor, SDT is expected to

https://doi.org/10.1021/acsomega.3c07445
ACS Omega 2024, 9, 1196−1205

have a clinical effect. Moreover, the specificity of SDT can also come from focused US exposure under image guidance, which can avoid off target effects. A detailed in vivo study is required to understand the systemic effects arising from the therapy and evaluate its therapeutic potential.

5. CONCLUSIONS

This study demonstrated the sonodynamic efficacy of porphyrin-based agents in vitro. Among the two sonosensitizers tested, the free base porphyrin derivative showed higher (60−70)% cell death relative to the agent with Zn metal conjugation (50% viability). ROS generation within the cells was found to be the mechanism of cell death. SDT not only caused cytotoxicity but also arrested proliferation of the treated cells. These findings demonstrate the SDT potential of carbohydrate-modified porphyrin-based sensitizers and support future in vivo studies to evaluate their therapeutic efficacy.

■ ASSOCIATED CONTENT

Supporting Information

The Supporting Information is available free of charge at https://pubs.acs.org/doi/10.1021/acsomega.3c07445.

Details of US power intensity settings in the transducer system against the measured values, emission spectrum of DPBF on subjecting to US exposure, MTT graph of cells exposed to US alone, and bright-field microscopy images of control groups from the wound healing assay (PDF)

■ AUTHOR INFORMATION

Corresponding Author

Manita Das − *Department of Electrical Engineering, Indian Institute of Technology (IIT) Gandhinagar, Gandhinagar, Gujarat 382355, India;* orcid.org/0009-0009-9843-9575; Email: manitadas1622@gmail.com

Authors

Vijayalakshmi Pandey − *Department of Chemistry, Indian Institute of Technology (IIT) Gandhinagar, Gandhinagar, Gujarat 382355, India*

Kuldeep Jajoria − *Department of Electrical Engineering, Indian Institute of Technology (IIT) Gandhinagar, Gandhinagar, Gujarat 382355, India*

Dhiraj Bhatia − *Department of Biological Engineering, Indian Institute of Technology (IIT) Gandhinagar, Gandhinagar, Gujarat 382355, India;* orcid.org/0000-0002-1478-6417

Iti Gupta − *Department of Chemistry, Indian Institute of Technology (IIT) Gandhinagar, Gandhinagar, Gujarat 382355, India;* orcid.org/0000-0003-4288-8661

Himanshu Shekhar − *Department of Electrical Engineering, Indian Institute of Technology (IIT) Gandhinagar, Gandhinagar, Gujarat 382355, India;* orcid.org/0000-0003-1226-4196

Complete contact information is available at: https://pubs.acs.org/10.1021/acsomega.3c07445

Notes

The authors declare no competing financial interest.

■ ACKNOWLEDGMENTS

M.D. thanks the Department of Biotechnology GoI for Postdoctoral fellowship. H.S. thanks the Department of Biotechnology GoI for Har Govind Khorana Innovative Young Biotechnologist Award.

■ REFERENCES

(1) Su, Y.; Pogash, T. J.; Nguyen, T. D.; Russo, J. Development and Characterization of Two Human Triple-Negative Breast Cancer Cell Lines with Highly Tumorigenic and Metastatic Capabilities. *Cancer Med.* **2016**, *5* (3), 558−573.

(2) Sporikova, Z.; Koudelakova, V.; Trojanec, R.; Hajduch, M. Genetic Markers in Triple-Negative Breast Cancer. *Clin. Breast Cancer* **2018**, *18* (5), e841−e850.

(3) Liu, X.; Wu, K.; Zheng, D.; Luo, C.; Fan, Y.; Zhong, X.; Zheng, H. Efficacy and Safety of PARP Inhibitors in Advanced or Metastatic Triple-Negative Breast Cancer: A Systematic Review and Meta-Analysis. *Front. Oncol.* **2021**, *11*, No. 742139.

(4) Tung, N.; Garber, J. E. PARP Inhibition in Breast Cancer: Progress Made and Future Hopes. *npj Breast Cancer* **2022**, *8* (1), 1−5.

(5) Perillo, B.; Di Donato, M.; Pezone, A.; Di Zazzo, E.; Giovannelli, P.; Galasso, G.; Castoria, G.; Migliaccio, A. ROS in Cancer Therapy: The Bright Side of the Moon. *Exp. Mol. Med.* **2020**, *52* (2), 192−203.

(6) Yang, H.; Villani, R. M.; Wang, H.; Simpson, M. J.; Roberts, M. S.; Tang, M.; Liang, X. The Role of Cellular Reactive Oxygen Species in Cancer Chemotherapy. *J. Exp. Clin. Cancer Res.* **2018**, *37* (1), 1−10.

(7) Roy, J.; Pandey, V.; Gupta, I.; Shekhar, H. Antibacterial Sonodynamic Therapy: Current Status and Future Perspectives. *ACS Biomaterials Science and Engineering.* **2021**, *7*, 5326.

(8) Yan, P.; Liu, L. H.; Wang, P. Sonodynamic Therapy (SDT) for Cancer Treatment: Advanced Sensitizers by Ultrasound Activation to Injury Tumor. *ACS Appl. Bio Mater.* **2020**, *3* (6), 3456−3475.

(9) Rengeng, L.; Qianyu, Z.; Yuehong, L.; Zhongzhong, P.; Libo, L. Sonodynamic Therapy, a Treatment Developing from Photodynamic Therapy. *Photodiagnosis Photodyn. Ther.* **2017**, *19* (June), 159−166.

(10) Borah, B. M.; Cacaccio, J.; Durrani, F. A.; Bshara, W.; Turowski, S. G.; Spernyak, J. A.; Pandey, R. K. Sonodynamic Therapy in Combination with Photodynamic Therapy Shows Enhanced Long-Term Cure of Brain Tumor. *Sci. Rep.* **2020**, *10* (1), 21791.

(11) Liu, Z.; Li, J.; Chen, W.; Liu, L.; Yu, F. Light and Sound to Trigger the Pandora's Box against Breast Cancer: A Combination Strategy of Sonodynamic, Photodynamic and Photothermal Therapies. *Biomaterials* **2020**, *232*, No. 119685.

(12) Liang, S.; Deng, X.; Chang, Y.; Sun, C.; Shao, S.; Xie, Z.; Xiao, X.; Ma, P.; Zhang, H.; Cheng, Z.; Lin, J. Intelligent Hollow Pt-CuS Janus Architecture for Synergistic Catalysis-Enhanced Sonodynamic and Photothermal Cancer Therapy. *Nano Lett.* **2019**, *19* (6), 4134−4145.

(13) Zheng, Y.; Ye, J.; Li, Z.; Chen, H.; Gao, Y. Recent Progress in Sono-Photodynamic Cancer Therapy: From Developed New Sensitizers to Nanotechnology-Based Efficacy-Enhancing Strategies. *Acta Pharm. Sin. B* **2021**, *11* (8), 2197−2219.

(14) Li, Q.; Liu, Q.; Wang, P.; Feng, X.; Wang, H.; Wang, X. The Effects of Ce6-Mediated Sono-Photodynamic Therapy on Cell Migration, Apoptosis and Autophagy in Mouse Mammary 4T1 Cell Line. *Ultrasonics* **2014**, *54* (4), 981−989.

(15) Kooiman, K.; Roovers, S.; Langeveld, S. A. G.; Kleven, R. T.; Dewitte, H.; O'Reilly, M. A.; Escoffre, J. M.; Bouakaz, A.; Verweij, M. D.; Hynynen, K.; Lentacker, I.; Stride, E.; Holland, C. K. Ultrasound-Responsive Cavitation Nuclei for Therapy and Drug Delivery. *Ultrasound Med. Biol.* **2020**, *46* (6), 1296−1325.

(16) Delaney, L. J.; Isguven, S.; Eisenbrey, J. R.; Hickok, N. J.; Forsberg, F. Making Waves: How Ultrasound-Targeted Drug Delivery Is Changing Pharmaceutical Approaches. *Mater. Adv.* **2022**, *3* (7), 3023−3040.

(17) Ahmed, S.; Davoust, E.; Savoie, H.; Boa, A. N.; Boyle, R. W. Thioglycosylated Cationic Porphyrins - Convenient Synthesis and Photodynamic Activity in Vitro. *Tetrahedron Lett.* **2004**, *45* (31), 6045−6047.

(18) Yano, S.; Hirohara, S.; Obata, M.; Hagiya, Y.; Ogura, S.-i.; Ikeda, A.; Kataoka, H.; Tanaka, M.; Joh, T. Current States and Future

Views in Photodynamic Therapy. *J. Photochem. Photobiol. C Photochem. Rev.* **2011**, *12* (1), 46−67.
(19) Singh, S.; Aggarwal, A.; Thompson, S.; Tomé, J. P. C.; Zhu, X.; Samaroo, D.; Vinodu, M.; Gao, R.; Drain, C. M. Synthesis and Photophysical Properties of Thioglycosylated Chlorins, Isobacteriochlorins, and Bacteriochlorins for Bioimaging and Diagnostics. *Bioconjugate Chem.* **2010**, *21* (11), 2136−2146.
(20) Hirohara, S.; Obata, M.; Ogata, S. I.; Ohtsuki, C.; Higashida, S.; Ogura, S. I.; Okura, I.; Takenaka, M.; Ono, H.; Sugai, Y.; Mikata, Y.; Tanihara, M.; Yano, S. Cellular Uptake and Photocytotoxicity of Glycoconjugated Chlorins in HeLa Cells. *J. Photochem. Photobiol. B Biol.* **2005**, *78* (1), 7−15.
(21) Pandey, V.; Raza, M. K.; Joshi, P.; Gupta, I. Synthesis of Water-Soluble Thioglycosylated Trans-A2B2Type Porphyrins: Cellular Uptake Studies and Photodynamic Efficiency. *J. Org. Chem.* **2020**, *85* (10), 6309−6322.
(22) Pandey, V.; Jain, D.; Pareek, N.; Gupta, I. Pd(II) Porphyrins: Synthesis, Singlet Oxygen Generation and Photoassisted Oxidation of Aldehydes to Carboxilic Acids. *Inorg. Chim. Acta* **2020**, *502* (Ii), No. 119339.
(23) Giuntini, F.; Foglietta, F.; Marucco, A. M.; Troia, A.; Dezhkunov, N. V.; Pozzoli, A.; Durando, G.; Fenoglio, I.; Serpe, L.; Canaparo, R. Insight into Ultrasound-Mediated Reactive Oxygen Species Generation by Various Metal-Porphyrin Complexes. *Free Radic. Biol. Med.* **2018**, *121*, 190−201.
(24) Ooyama, Y.; Enoki, T.; Ohshita, J.; Kamimura, T.; Ozako, S.; Koide, T.; Tani, F. Singlet Oxygen Generation Properties of an Inclusion Complex of Cyclic Free-Base Porphyrin Dimer and Fullerene C60. *RSC Adv.* **2017**, *7* (30), 18690−18695.
(25) Entradas, T.; Waldron, S.; Volk, M. The Detection Sensitivity of Commonly Used Singlet Oxygen Probes in Aqueous Environments. *J. Photochem. Photobiol., B: Biol.* **2020**, *204*, No. 111787.
(26) Yesilgul, N.; Uyar, T. B.; Seven, O.; Akkaya, E. U. Singlet Oxygen Generation with Chemical Excitation of an Erythrosine-Luminol Conjugate. *ACS Omega* **2017**, *2* (4), 1367−1371.
(27) Xu, H. N.; Chen, H. J.; Zheng, B. Y.; Zheng, Y. Q.; Ke, M. R.; Huang, J. D. Preparation and Sonodynamic Activities of Water-Soluble Tetra-α-(3-Carboxyphenoxyl) Zinc(II) Phthalocyanine and Its Bovine Serum Albumin Conjugate. *Ultrason. Sonochem.* **2015**, *22*, 125−131.
(28) Lutkus, L. V.; Rickenbach, S. S.; McCormick, T. M. Singlet Oxygen Quantum Yields Determined by Oxygen Consumption. *J. Photochem. Photobiol. A Chem.* **2019**, *378* (March), 131−135.
(29) Gradova, M. A.; Gradov, O. V.; Lobanov, A. V.; Bychkova, A. V.; Nikolskaya, E. D.; Yabbarov, N. G.; Mollaeva, M. R.; Egorov, A. E.; Kostyukov, A. A.; Kuzmin, V. A.; Khudyaeva, I. S.; Belykh, D. V. Characterization of a Novel Amphiphilic Cationic Chlorin Photosensitizer for Photodynamic Applications. *Int. J. Mol. Sci.* **2023**, *24* (1), 345.
(30) Kirar, S.; Chaudhari, D.; Thakur, N. S.; Jain, S.; Bhaumik, J.; Laha, J. K.; Banerjee, U. C. Light-Assisted Anticancer Photodynamic Therapy Using Porphyrin-Doped Nanoencapsulates. *J. Photochem. Photobiol. B Biol.* **2021**, *220* (March), No. 112209.
(31) Vallecorsa, P.; Di Venosa, G.; Ballatore, M. B.; Ferreyra, D.; Mamone, L.; Sáenz, D.; Calvo, G.; Durantini, E.; Casas, A. Novel Meso-Substituted Porphyrin Derivatives and Its Potential Use in Photodynamic Therapy of Cancer. *BMC Cancer* **2021**, *21* (1), 1−12.
(32) Lafond, M.; Yoshizawa, S.; Umemura, S.-i Sonodynamic Therapy: Advances and Challenges in Clinical Translation. *J. Ultrasound Med.* **2019**, *38* (3), 567−580.
(33) Araújo Martins, Y.; Zeferino Pavan, T.; Fonseca Vianna Lopez, R. Sonodynamic Therapy: Ultrasound Parameters and in Vitro Experimental Configurations. *Int. J. Pharm.* **2021**, *610*, No. 121243.
(34) Liu, X.; Pan, X.; Wang, C.; Liu, H. Modulation of Reactive Oxygen Species to Enhance Sonodynamic Therapy. *Particuology* **2023**, *75*, 199−216.
(35) Son, S.; Kim, H.; Wang, X.; Zhang, C.; Yoon, S. A.; Shin, J.; Sharma, A.; Lee, M. H.; Cheng, L.; Wu, J.; Kim, J. S. Multifunctional Sonosensitizers in Sonodynamic Cancer Therapy. *Chem. Soc. Rev.* **2020**, *49*, 3244−3261, DOI: 10.1039/c9cs00648f.
(36) Rosenthal, I.; Sostaric, J. Z.; Riesz, P. Sonodynamic Therapya Review of the Synergistic Effects of Drugs and Ultrasound. *Ultrason. Sonochem.* **2004**, *11* (6), 349−363.
(37) Hwang, E.; Yun, M.; Jung, H. S. Mitochondria-Targeted Organic Sonodynamic Therapy Agents: Concept, Benefits, and Future Directions. *Front. Chem.* **2023**, *11* (June), 1−13.
(38) Canavese, G.; Ancona, A.; Racca, L.; Canta, M.; Dumontel, B.; Barbaresco, F.; Limongi, T.; Cauda, V. Nanoparticle-Assisted Ultrasound: A Special Focus on Sonodynamic Therapy against Cancer. *Chem. Eng. J.* **2018**, *340*, 155−172.
(39) Fan, C. H.; Wu, N.; Yeh, C. K. Enhanced Sonodynamic Therapy by Carbon Dots-Shelled Microbubbles with Focused Ultrasound. *Ultrason. Sonochem.* **2023**, *94*, No. 106342.
(40) Maqbool, M.; Bekele, F.; Fekadu, G. Treatment Strategies Against Triple-Negative Breast Cancer: An Updated Review. *Breast Cancer Targets Ther.* **2022**, *14*, 15−24.
(41) Shin, E.; Koo, J. S. Glucose Metabolism and Glucose Transporters in Breast Cancer. *Front. Cell Dev. Biol.* **2021**, *9*, No. 728759.

https://doi.org/10.1021/acsomega.3c07445
ACS Omega 2024, 9, 1196−1205